Single-shot, high sensitivity X-ray phase contrast imaging system based on a Hartmann mask

Ombeline de La Rochefoucauld[1], Ginevra Begani Provinciali[2,3], Alessia Cedola[2], Mourad Idir[4], Guillaume Dovillaire[5], Fabrice Harms[5], Jérôme Legrand[5], Xavier Levecq[5], Francesca Mastropietro[6], Lionel Nicolas[5], Laura Oudjedi[1], Martin Piponnier[1], Philippe Zeitoun[3]

[1]Imagine Optic, rue François Mitterrand, 33400 Talence, France, odlrochefoucauld@ imagine-optic.com
[2]CNR-Institute of Nanotechnology, c/o Physics Department "Sapienza" University, Piazzale Aldo Moro 5 00185 Rome, Italy
[3] Laboratoire d'Optique Appliquée, CNRS, ENSTA ParisTech, IP Paris, 828 boulevard des Maréchaux, Palaiseau, France
[4]Brookhaven National Laboratory, NSLS-II, NY, USA
[5]Imagine Optic, 18 rue Charles de Gaulle, 91400 Orsay, France
[6]Institut Bergonié, 229 cours de l'Argonne, 33000, Bordeaux, France

Abstract

Significant efforts are currently ongoing in X-Ray imaging to provide multimodal imaging systems, targeting better sensitivity and specificity for both biomedical or non-destructive testing (NDT) applications. X-Ray Phase Contrast Imaging (X-PCI) shows great capability to differentiate elements with similar absorption. For example, in the medical field, knowing the chemical composition of breast microcalcifications would help to differentiate malign and benign tumors. The composition can be determined from the measurement of the phase as the optical index of materials is directly related to the composition. We propose a novel, high-sensitivity X-ray quantitative phase imaging system based on a Hartmann wavefront sensor. The system provides high resolution (20µm without magnification) and high sensitivity (~100 nrad), and is compatible with tomographic experiments using both synchrotron beamlines or laboratory sources. We present here our first X-PCI prototype as well as the first images obtained. We also present an alternative design based on the same approach, providing larger field-of-view at the cost of some trade-off regarding resolution and sensitivity and the first tomographic results obtained with this imaging system.

Keywords: X-ray, phase contrast imaging, Hartmann, wavefront sensing

1 Introduction

X-ray imaging is an essential tool for non-invasive control of various samples, both for biomedical diagnosis and non-destructive testing. When the absorptions are very similar between two components of a sample, it becomes difficult to differentiate them using X-ray absorption imaging. However, it is still possible to disentangle the components by measuring the induced variations of the phase of the X-ray beam. This is the basic of X-ray Phase Contrast Imaging (X-PCI). For most technics, X-PCI aims at providing clear images of samples that are normally unresolvable with amplitude imaging. However, it is possible to extract more information about the sample by reminding that the phase is linked to the decrement of the real part of the refractive index, called δ, of each component (while the absorption is related to the imaginary part, called β).

Different X-PCI imaging approaches have already been proposed and characterized [1-4]. We propose here a phase imaging system based on a Hartmann mask that will provide quantitative phase images where most existing technics give only qualitative images.

2 Phase Imaging System with a Hartmann sensor

2.1 Phase Imaging Principle

Let's consider a plane wave, propagating along the z-direction through a medium with refractive index, $n = 1 - \delta + i\beta$ and wave vector k:

$$\Psi(z) = \Psi_0 e^{-inkz} = \Psi_0 e^{-i(1-\delta+i\beta)kz} = \Psi(z_0) e^{-i\delta kz} e^{-\beta kz}$$

When passing through a sample of thickness d, the amplitude of the wave is attenuated by a factor $e^{-\beta k d}$ and the phase is shifted by the quantity $\delta k d$. The sample modifies locally the wavefront, leading to the local refraction of the wave by an angle α. α corresponds to the local wavefront slope, i.e. the local gradient of the wavefront.

The Hartmann sensor is a device that is commonly used for wavefront sensing [5-8]. It is composed of a grid of regularly spaced holes and a detector placed some distance away. Each hole in the mask generates a bright spot on the camera (Fig. 1a). To determine the wavefront of the incoming wave, two images are needed. The first one is taken without the sample (Fig. 1a). It is a calibration measurement to get the reference position of the spots. The second image is taken with the sample that will locally refract the wave, yielding to local shift of the spots (Fig. 1b). For both images, position and amplitude of each spot are measured.

The ratio of the sample to reference amplitudes gives the absorption of the sample. The difference between the new and the reference positions (Δy in Fig. 1b) is proportional to the angle of refraction ($\tan(\alpha) = \Delta y/L$), i.e. the 2D gradient of the wavefront relatively to the reference beam.

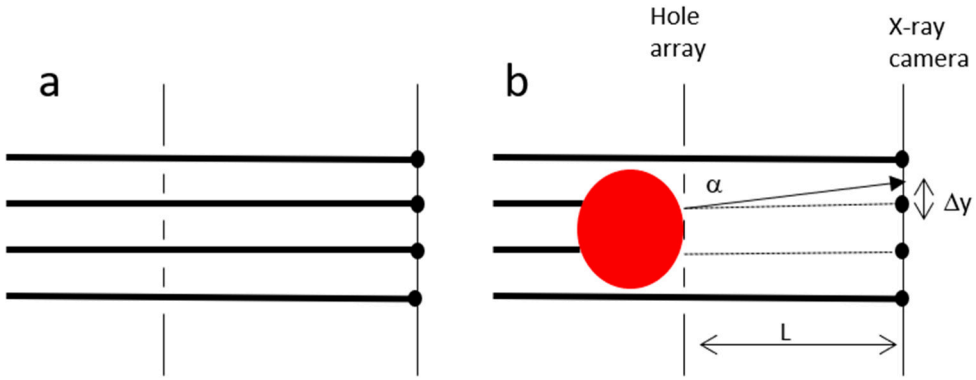

Figure 1. Schematic description of a Hartmann wavefront sensor. a) The reference wave (without sample) creates sub-images on the detector. b) When passing through a sample, the wavefront is modified, resulting in a displacement (Δy) of the sub-images on the detector. α is the angle of refraction.

Measurements of local small angular deviations (Δx, Δy) allow retrieving the angle of refraction (α_x and α_y) and therefore the 2D gradient of the wavefront. An integration of the wavefront along X and Y directions determines the phase. Therefore, a wavefront sensor generates a phase map.

The main advantages of the Hartmann approach are: 1) 2D images are acquired from one acquisition; 2) single exposure: with only one acquisition, we measure both the absorption and deflection, 3) achromatic: the system is designed to keep high sensitivity over a wide energy range; 4) compatible with tomography.

2.2 Small Field of View prototype

The first phase imaging prototype we developed is shown Fig. 2. The system is composed of a Hartmann mask, a scintillator, a relay lens and a CCD camera. The mask is based on an array of holes regularly spaced, drilled on a gold substrate. The incoming X-ray light is diffracted by the holes and propagates up to the scintillator. The scintillator converts X-rays to visible light that is then collected by the relay lens and imaged onto the CCD camera. This first design has been optimized for an energy range of 5 to 25 keV. It provides a field of view of few mm². The spatial sampling is 20µm. The sensor theoretical performances are a dynamic range of +/- 60 µrad and a sensitivity of 70 nrad.

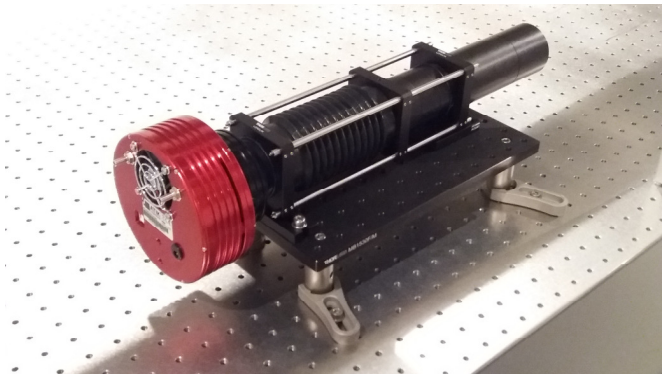

Figure 2. Picture of the first phase imaging prototype. The system is 50 cm long.

2.3 Larger Field of View Prototype

It is possible to adjust the design parameters of the setup in order to increase the field of view (FoV) up to several centimeters, at the cost of a slight reduction of the sensitivity.

The second prototype, allowing a FoV of few centimeters is presented Fig. 3. A 3*3 cm² mask of holes is positioned in front of a flat panel (Xineos 2329 from Teledyne Dalsa) of dimensions 23*29 cm². In this configuration, the size of the mask is the limiting parameter for the FoV. The system has 2-5 µrad phase sensitivity and 50µm spatial resolution (without magnification).

Figure 3: The phase imaging system based on a Hartmann mask and a flat panel.

3 Results and Discussion

To demonstrate the interest of the Hartmann approach for phase imaging, we first used 120µm diameter nylon fibers as phase objects and a hex key as absorption object (Fig. 4a). The small FoV system was placed at 60cm away from an Excillum Metaljet high brilliance microfocus X-ray source, having a K-α emission around 9 keV. The sample was placed between the source and the system, at roughly 30cm from the Hartmann mask. The raw image is presented on Fig. 4b, with a zoom (Fig. 4c) that shows the bright spots.

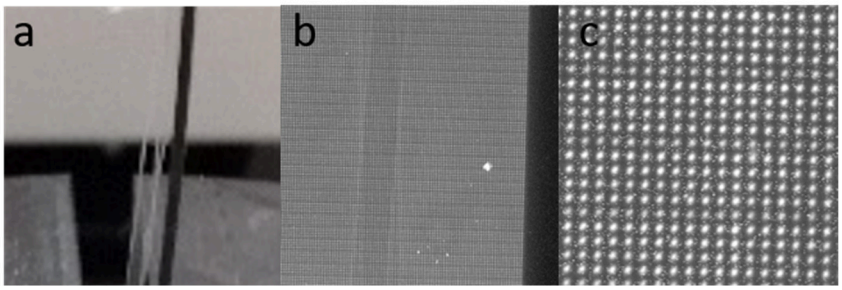

Figure 4: a) Sample composed of two crossing nylon fibers and a hex key as an absorption object; b) Raw image where the nylon fibers cross; the black part on the right corresponds to the hex key; c) zoom on the raw image to illustrate the bright spots

Figure 5 illustrates the absorption and deflections generated by the samples and measured by the system, with a resolution of 10µm per pixel. If we look at the nylon fibers, we observe no deflection along the Y direction but deflections along the X direction of about 10µrad and absorption of roughly 10% per nylon fiber. If we look at the hex key border, we can observe a total absorption (preventing to measure the deflection).

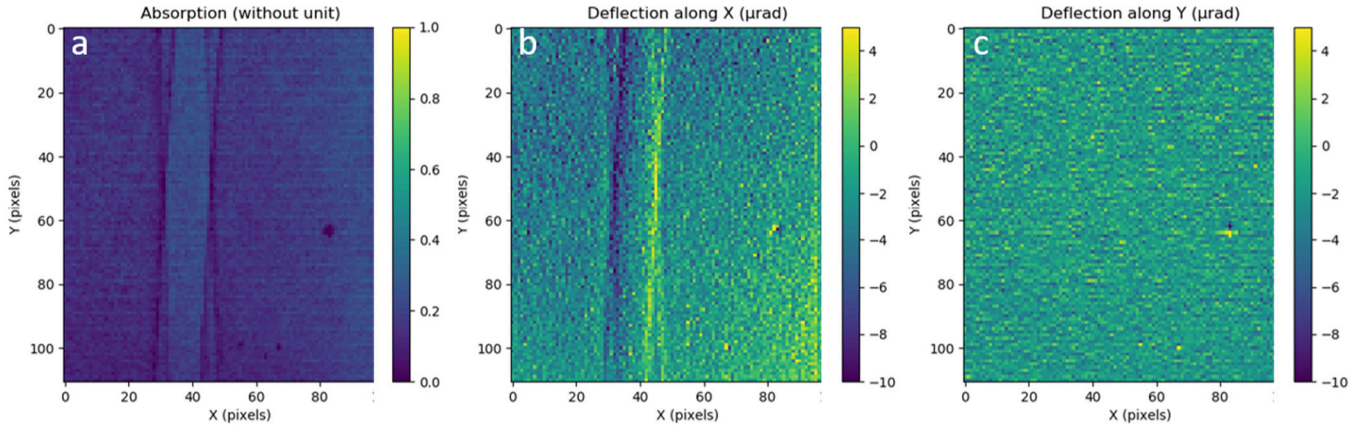

Figure 5: a) Measured absorption (a.u): yellow corresponds to a maximal absorption. b) Measured deflection along X (µrad), c) Measured deflection along Y (µrad).

Figure 6 presents results obtained with the second prototype (Fig. 3), allowing a larger FoV. The experimental set-up is composed of the Excillum Metaljet high brilliance microfocus X-ray source, the Hartmann mask and the Flat panel Xineos 2329 (Teledyne Dalsa).

We used two Eppendorf tubes, one filled with immersion oil for microscope and the other one with water (Fig.6a). The mask was placed at 50cm from the microfocus X-ray source. The samples were placed between the source and the mask, at~1cm from the mask. The raw image and a zoom are presented Fig. 6b-c.

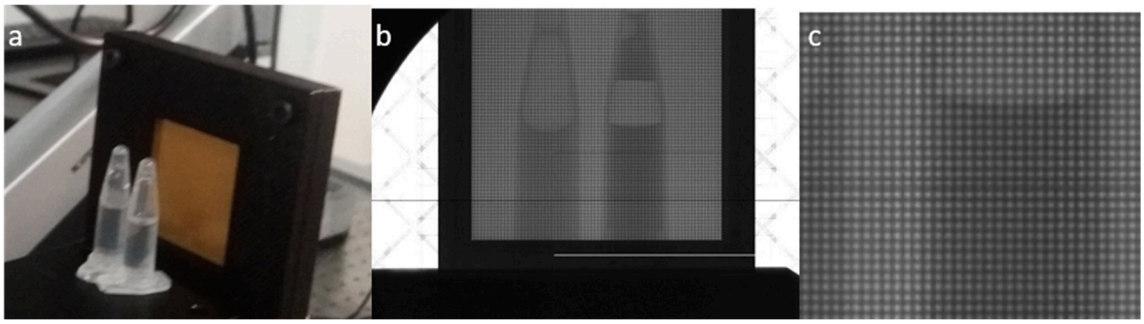

Figure 6: a) Picture of the two Eppendorf tubes in front of the mask; b) raw image c) zoom on the raw image

The position and amplitude of each spot were calculated on the images taken with and without the tubes. The ratio of the amplitudes gives the absorption of the sample (Fig. 7a) and the difference of position is proportional to the deflection generated by the sample (Fig. 7b). We can clearly observe deflections in the X direction up to +/-6µrad and absorption of roughly 25% for the oil and 35% for the water (Fig. 7c-d). The noise level is ~1µrad P-V.

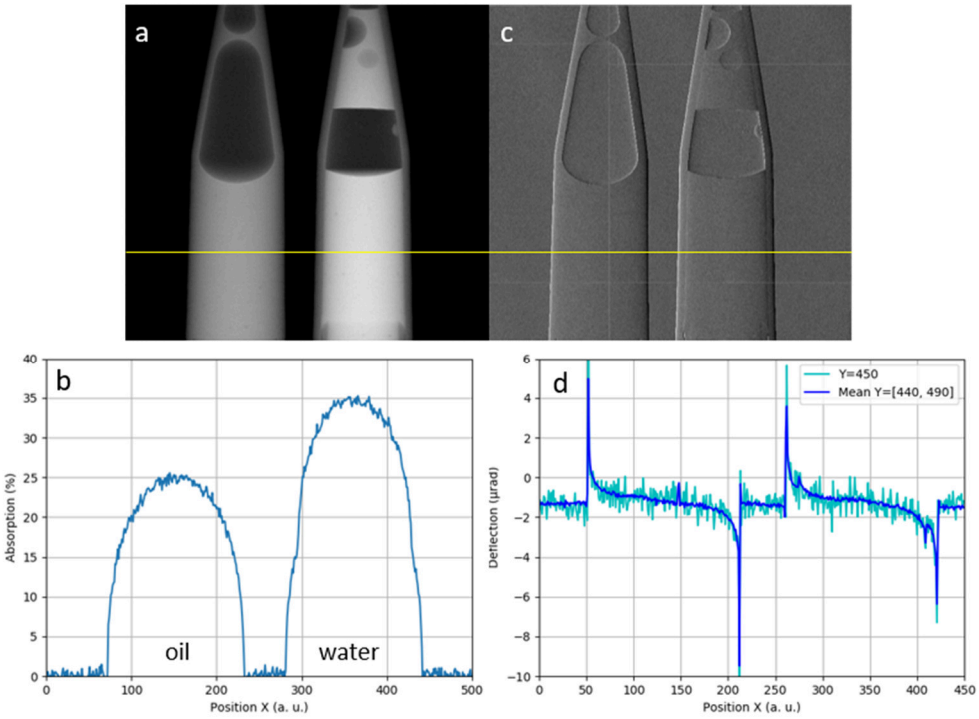

Figure 7: The sample with oil is on the left, the one with water on the right. a) Intensity map (from 0 to 40%); b) and corresponding profile along the yellow line (cyan) and the mean around the yellow line (in blue). c) Deflection along X (from -5 to 5µrad) and d) corresponding profile.

4 First Steps toward tomography

We performed a first tomographic experiment on a reference sample composed of three tubes: one was a tube of carbon (1.5mm in diameter), one was a tube of PMMA (2mm in diameter) and the third one was a 2mm diameter polycarbonate tube filled with 150µm spheres of soda lime glass (Fig. 8a). The sample was situated at 22 cm from the Excillum microfocus X-ray source. The large FoV Hartmann mask was located at a distance of ~44 cm from the source. In this optical configuration, the theoretical spatial resolution on the sample was about 25µm with 1.5 cm of field of view. Images were acquired with the Xineos 2329 flat panel. 400 projections were taken. The image on Fig. 8b represents a 2D absorption image (similar to Fig. 7a). Around 9 keV, PMMA and carbon have similar absorption, and thus are not that easy to distinguish with conventional absorption images.

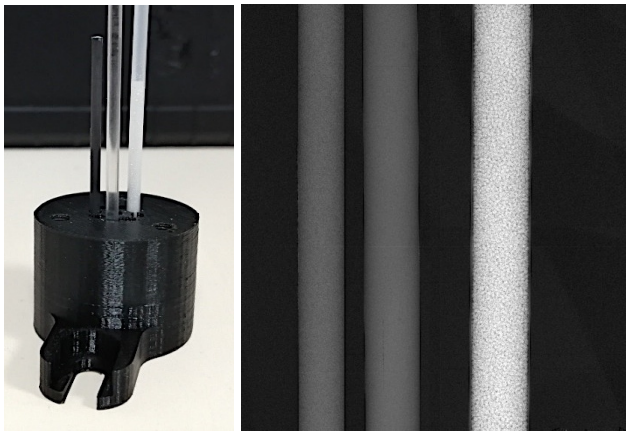

(a) (b)

Figure 8: (a) Picture of the tubes used for the 9keV tomography experiment. One was a tube made of carbon (1.5mm in diameter), one was a tube of PMMA (2mm in diameter) and the third one is a 2mm diameter polycarbonate tube filled with 150µm spheres of

soda lime glass. (b) Radiography (axial view), i.e. absorption image, of three tubes achieved at energy of about 9 keV. The tube on the left is the carbon one, at the center the PPMA and on the right the one filled with microspheres.

From the 400 projections, 3D tomographic reconstruction was performed. For each projection, the absorption and deflection images were obtained (similar to Figs. 7a-c) and then combined. The resulting absorption image is presented on Fig. 9 as well as deflection image (projection along the Y-axis) on Fig. 10. The images Figs. 9a and 10a are showing a horizontal slide of the three tubes that are placed vertically on Figs. 8 and 9b. This result shows the potentiality of our wavefront sensors to be used on tomographic setups. However, these results are still preliminary and more work is needed to remove the artefacts from the reconstructed images.

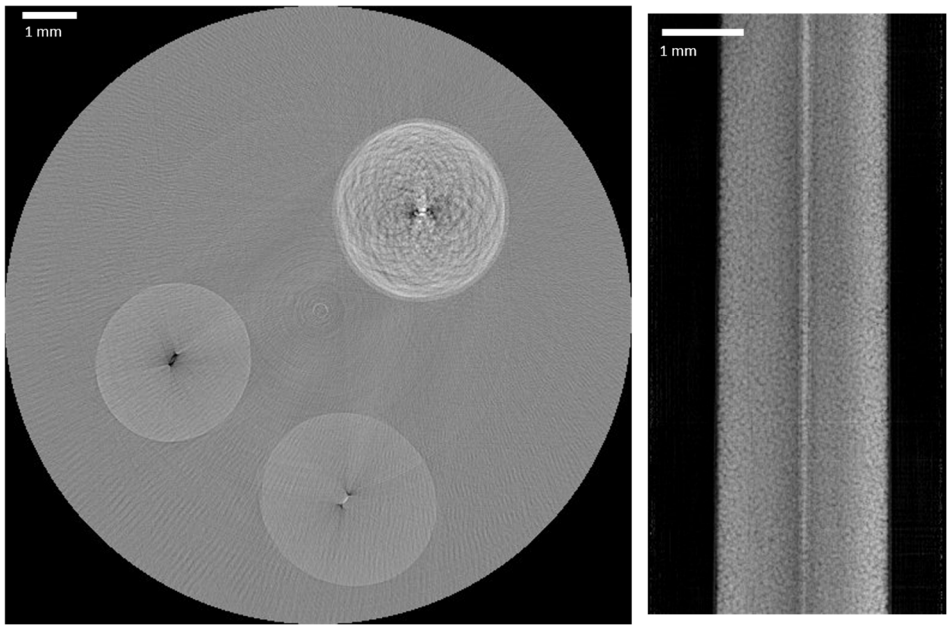

(a) (b)

Figure 9: Absorption 3D image: axial view on the 3 tubes (a) and coronal view (b) of the tube filled with micro-spheres.

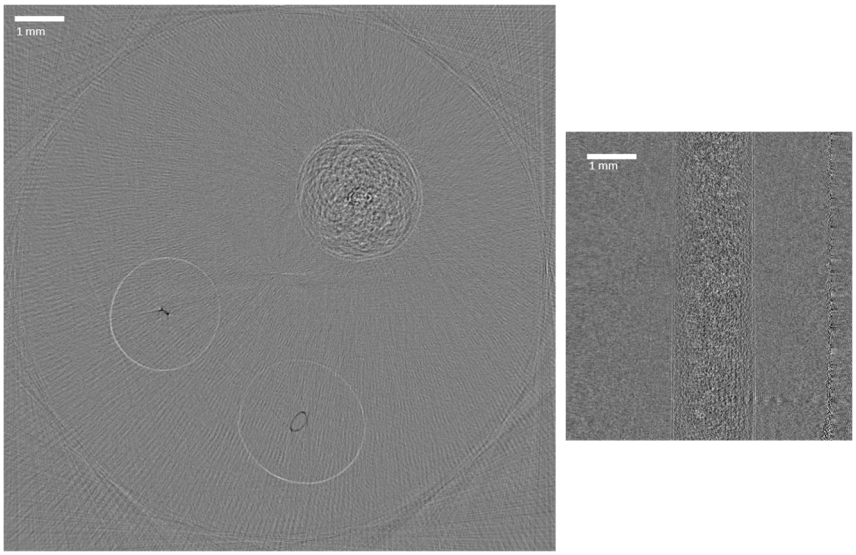

(a) (b)

Figure 10: Y-axis deflection 3D image: axial view on the 3 tubes (a) and coronal view (b) of the tube filled with micro-spheres. The edges of the tubes appear whiter due to peak of deflexion. The microspheres scattered the X-rays giving an apparent random deflexion.

5 Conclusion

Imagine Optic explored the ability of wavefront sensors to perform X-ray phase imaging associated with user-friendly software. The first prototype, with its small field of view (few mm^2) and high sensitivity (100 nrad) is compatible with small low-density object imaging. The second prototype has several cm^2 of field of view and 2-5µrad of sensitivity depending on the designs. Further characterization and optimization of the imaging systems are conducted.

As a conclusion, the main advantages of the Hartmann approach are: 1) 2D images are acquired from one acquisition; 2) the determination of absorption and phase from only one acquisition; 3) achromaticity; 4) compatible with tomography (as illustrated by Figs. 9-10). Therefore, our approach provides a simple alternative to already proposed X-PCI methods, either based on costly optical elements such as gratings or requiring the acquisition of multiple images to provide a single X-PCI image. Moreover, our system demonstrated its ability to provide quantitative phase images.

Acknowledgements

This work was funded by the Région Nouvelle-Aquitaine and the European Union FEDER under the XPULSE project: "development of an imaging system using X-rays based on ultra-short intense laser for applications in breast cancer imaging". We acknowledge ALPhANOV for giving us access to their X-ray source setup.

References

[1] Bravin, A., Coan P. and Suortti, P., X-ray phase-contrast imaging: from pre-clinical applications towards clinics", Phys. Med. Biol. 58, (2013), R1-R35

[2] Olivo Aet al., Low-dose phase contrast mammography with conventional x-ray sources, Med. Phys. 40 (9), (2013)

[3] Krejci F, Jakubek J, Kroupa M. "Hard x-ray phase contrast imaging using single absorption grating and hybrid semiconductor pixel detector". Rev. Sci. Instrum. 81, 113702. (2010)

[4] Wilkins SW, Nesterets YI, Gureyev TE, Mayo SC, Pogany A, Stevenson AW., "On the evolution and relative merits of hard X-ray phase-contrast imaging methods" Phil. Trans. R. Soc. A 372, (2014)

[5] Le Pape S., Zeitoun P., Idir M., Dhez D, Rocca J. J., François M., "Wavefront measurement in the soft X-ray range "Eur. Phys. J. AP, 20, 197 (2002)

[6] Le Pape S., Zeitoun P., Idir M., Dhez P., Rocca J; Francois, M., "Electromagnetic-field distribution measurements in the soft x-ray range: full characterization of a soft x-ray laser beam" Physical Review Letters, 88, Numéro 18, 2002

[7] Mercère, P., Zeitoun, P., Idir, M., Le Pape, S., Douillet, D., Levecq, X., Dovillaire, G., Bucourt, S.Goldberg, K.A., Naulleau, P. P. and Rekawa, S., "Hartmann wave-front measurement at 13.4 nm with λ_{EUV}/120 accuracy," Opt. Lett. **28**(17), 1534 (2003).

[8] de La Rochefoucauld O. et al, "Developments of EUV/X-ray wavrefront sensors and adaptive optics at Imagine Optic", Proc. SPIE 10761, Adaptive X-Ray Optics V, 107610E (2018)